THE JOURNAL OF PHYSICAL CHEMISTRY C

Feature Article

pubs.acs.org/JPCC

Kinetic and Thermodynamic Modified Wulff Constructions for Twinned Nanoparticles

Emilie Ringe,*[,†,§] Richard P. Van Duyne,[†] and Laurence D. Marks[‡]

[†]Department of Chemistry, Northwestern University, 2145 Sheridan Road, Evanston, Illinois 60208, United States

[‡]Department of Materials Science and Engineering, Northwestern University, 2220 Campus Drive, Evanston, Illinois 60208, United States

Supporting Information

ABSTRACT: Wulff constructions are a powerful tool to predict the shape of nanoparticles, which strongly influences their performance in catalysis, sensing, and surface-enhanced spectroscopies. Previous Wulff models focused on energy minimization and included contributions from the surface energy, interface energy, twin boundaries, and segregation-induced bulk energy changes. However, a large number of shapes cannot be understood by such thermodynamic approaches, in particular many of the twinned late transition metal (Ag, Au, Pt, Pd, etc.) particles of interest in catalysis and plasmonics. A review of the modified Wulff (i.e., twinned) construction is presented here, followed by the development of a modified kinetic Wulff model, which, by including kinetic parameters, explains the emergence of commonly observed shapes such as bitetrahedra, truncated bitetrahedra, thin triangular platelets, perfect decahedra, and decahedral rods.

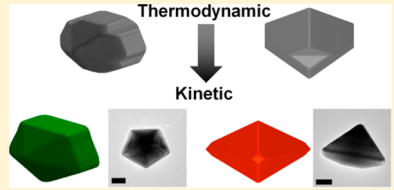

INTRODUCTION

The shape, surface, and internal structure of nanoparticles are topics of continuing interest due to their use in a range of both current and future technologies, ranging from catalysis to plasmonic and biomedical applications, in addition to the continuing importance of buried nanoparticles (precipitates) within materials leading to improved properties. While the last decades have seen substantial strides in synthetic methods aimed at making nanoparticles of a desired shape in high yields, understanding of the growth details has lagged behind the synthesis in many respects. It is often unclear whether a particular shape/structure is produced because of the thermodynamics or kinetics of growth, and what quantitatively rather than qualitatively are the effects of factors such as solution concentration, surfactants, and surface chemisorbed species.

Thermodynamic modeling of the shape of single crystals is over a century old: in 1873, Gibbs[1−3] first proposed that the lowest energy shape of a droplet is determined by a surface energy minimization. Based upon the initial observations of Wulff[4] about solids, this evolved into the so-called "Wulff construction" which states that the normal vector length to any external face is proportional to the surface free energy. The first formal proof of this was given by von Laue,[5] generalized to curved surfaces by Dinghas,[6] with Herring[7] giving some important further analysis. An extension for supported particles on a flat substrate was described by Winterbottom,[8] extended to an edge by Zia et al. in what they called the SummerTop construction.[9] A more recent addition has been for alloy nanoparticles.[10]

However, not all nanoparticles are single crystals. Since the seminal work of Ino and Ogawa[11−13] and the later work of Allpress and Sanders,[14] it has been known that nanoparticles of gold, silver, and other face-centered cubic (fcc) metals can have rather unusual structures. Dark field electron microscopy studies[11−13] showed that icosahedral (Ic) and decahedral (Dh) structures existed, which were called multiply twinned particles (MTPs). Regular single crystals (such as tetrahedra) and particles with one or more parallel twin boundaries (laminar twinned particles or LTPs) were also observed. The MTPs could be described as assemblies of tetrahedral subunits, elastically strained by ∼2% for the Dh and ∼6% for the Ic to form space-filling structures. This interpretation was confirmed using lattice imaging[15] and later by atomic resolution imaging.[16,17] For completeness, we note that there are many other complicated shapes such as what were called "poly-particles" which are either polyicosahedral structures similar to those first analyzed by Hoare and Pal,[18] or partially coalesced particles.

The initial energetics study[13] of particle shape used a homogeneous strain model coupled with a surface energy analysis of the regular structures to show that the Ic particles were stable at small sizes. However, no adequate explanation was found for the stability of the Dh or other experimentally observed structures such as octahedra and tetrahedra. Later, the surface structure of the particles was generalized using a variant of the Wulff construction appropriate for twinned nanoparticles, called a modified Wulff construction.[19,20] Finally, by coupling the modified Wulff shapes with a disclination strain model for the Dh particles[21] and a three-dimensional variant for the Ic particles,[22] the existence of the Dh particles up to intermediate sizes was rationalized. Some strain relief

Received: February 13, 2013
Revised: April 18, 2013
Published: May 30, 2013

   dx.doi.org/10.1021/jp401566m | J. Phys. Chem. C 2013, 117, 15859−15870

mechanisms, which have generally been confirmed over the years, were also suggested.[23]

As a general formulation, which will be returned to later in a different form, the thermodynamic stability of MTPs can be considered in terms of the weighted surface energy of the two regions R_1 and R_2 of the standard stereographic triangle for an fcc material, as illustrated in Figure 1. In this triangle, R_1 and R_2

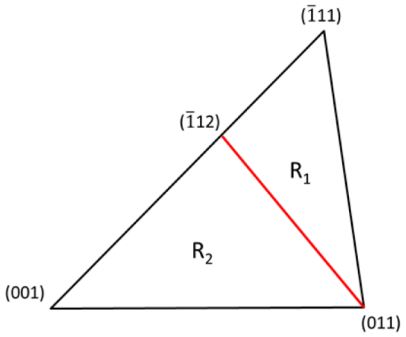

Figure 1. The two sections of the stereographic triangle associated with the relative thermodynamics as well as kinetics of MTPs, as discussed in the text.

are the projections of the regions selected by the presence (or absence) of twin planes, such that different twinning patterns result in different ratios of such regions: single crystals have an equal number of R_1 and R_2 ($48R_1$ and $48R_2$), decahedral MTPs have more R_1 ($60R_1$ and $40R_2$), and icosahedral MTPs have only R_1 (120). As the relative integrated surface energy of R_1 versus R_2 is dependent on the stability of {111} faces (as well as other facets), lower {111} surface free energy (versus {100}), such as in the presence of relevant chemisorbed species, is a sufficient condition for MTPs to be stable at small sizes. At larger sizes, as first pointed out by Ino, they cannot be thermodynamically stable because of the additional strain energy.[21,22]

Atomistic calculations have confirmed the stability of Ic and Dh particles, and specifically the modified Wulff solution which leads to a decahedron with re-entrant surfaces at the twin boundary,[24−26] probably the only known case of a thermodynamic minimum-energy shape which is nonconvex. The structure with just {111} and {100} facets has become known as the Marks decahedron.[27] Technically, this is only one specific case of the modified Wulff solution: star decahedra and short pentagonal rods are also solutions obeying the thermodynamic criteria of the preceding paragraph or the corresponding kinetic condition, as will be discussed later.

How these MTPs were formed was an early question; for instance, Allpress and Sanders[14] suggested assemblage of tetrahedral units in their original work. Whether the particles were frozen variants of 1−2 nm seeds which just grew larger or could change shape to follow the thermodynamic path of lowest energy was unclear. Yagi et al.[28] demonstrated through in situ experiments that such shape changes could occur, later confirmed by Iijima and Ichihashi.[29] While there were initially some questions as to the role of electron-beam heating or core excitations in the experiments, a more general explanation by Ajayan et al.[30−33] indicated that the activation energy for transformations between structures was relatively modest, similar to the energy landscape model for much smaller clusters developed by Berry and co-workers.[34−36] Ajayan et al.[31] also speculated that there should be a size−temperature phase diagram for nanoparticles.

Much of the early work has been reviewed[37] with earlier work on more diverse nanoparticles (called at that time "small particles" or "ultrafine particles") available in the argon-smokes literature.[38] More recent reviews are also available.[27,39] Given the growth of nanotechnology in the last decades, significant advances in synthesis and characterization methods have been made, for example, the discovery of new shape-control strategies,[40,41] attempts to measure nanoparticle phase maps,[30,32,42,43] as well as more precise structural characterization using aberration corrected TEM or X-ray methods. Modeling advances have accompanied experimental progress, for example, better elasticity models[44,45] and atomistic methods exploiting DFT.[42] However, no general models for the effects of growth kinetics on shape are currently available, and many recent papers have presented results that could benefit from theoretical shape modeling, both kinetic and thermodynamic.

This paper has three main parts. The first is a rigorous background on the foundation of the thermodynamic and kinetic Wulff construction. Then, a short review of the modified Wulff construction is presented, with examples of contemporary twinned structures (such as star decahedra) experimentally observed but not previously modeled. The limitations of this thermodynamic model, in particular its inability to explain many commonly synthesized structures, will be discussed.

The third part presents a new kinetic model inspired by the modified Wulff construction and the kinetic Wulff construction.[46−49] The latter dates back to the early work of Frank[46] and in various forms has been used for continuum single crystal growth.[50−52] In the current modified kinetic Wulff model, growth-assisting defects such as re-entrant surfaces and disclinations/twin boundaries are mathematically taken into account and discussed. This new model gives quasi-stationary solutions for most if not all the structures not explained by the thermodynamic models as well as shapes commonly found for fcc nanoparticles. This approach works equally well for gas and liquid phase growth; simple implementation (graphical user interface available in the Supporting Information) and fast computation time make it a useful tool to predict shapes for large (>5 nm) particles, where atomistic methods (DFT, for instance) are limited by computing power. While no explicit solutions for other crystallographies are presented, these can be generated without difficulty.

The paper concludes with an overview of the model limitation and possible expansions, as well as a brief discussion of shape instabilities and transformations.

METHODS

All the calculations necessary to produce geometrical models presented herein (Figures 3−5) were performed in MATLAB by calculating a growth front value (using the growth velocities and enhancements described in eqs 18 and 19) at each point in a square three-dimensional mesh, and then producing an isosurface linking all points with the same value. A detailed explanation of the code and the code itself are provided in the Supporting Information. A graphical user interface was developed to model nanoparticle shape; it includes both single crystal and modified Wulff constructions, thermodynamic and kinetic. The user interface as well as associated documentation is provided as Supporting Information. The parameters used for Figures 3−5 are reported in Table S1 and S2 of the Supporting Information. Particles shown in Figure 6 were the product of

dx.doi.org/10.1021/jp401566m | J. Phys. Chem. C 2013, 117, 15859−15870

the reduction of hydrogen tetrachloroaurate ($HAuCl_4$) in a polyol synthesis in the presence of PVP (poly(vinyl pyrrolidone)).[53−55]

THERMODYNAMIC AND KINETIC WULFF CONSTRUCTIONS

In this first part, the transition from atomistic to continuum description of matter will be sketched, as the kinetic and thermodynamic Wulff constructions are limits of this transition. We will also clarify the important distinction between kinetic and thermodynamic modeling, as well as discuss previous approaches. While many of the components are available in the literature, some generalizations are useful particularly in order to connect to ab initio thermodynamics (e.g., refs 56 and 57).

In a purely atomistic description, the total energy of an ordered, crystalline nanoparticle can be written as

$$E = \sum_{i,j,k} a_{ijk} n_i n_j n_k + \sum_{i,j} b_{ij} n_i n_j + \sum_i c_i n_i + d + \cdots \quad (1)$$

where the n_i are positive integers that represent the number of atoms along particular directions. In principle, the equation can be extended to include terms with inverse powers, but this is rarely useful. Assuming convex shapes for all single crystal regions and replacing eq 1 with a vector of normal distances for each face from a common origin $\underline{h} = (h_1, h_2, ..., h_k)$ for k facets, with all h_i real but not necessarily positive numbers, leads to

$$E = \sum_{i,j,k} A_{ijk} h_i h_j h_k + \sum_{i,j} B_{ij} h_i h_j + \sum_i C_i h_i + D + \cdots \quad (2)$$

As illustrated in Figure 2, each h_i is a combination of a geometric distance such as that from the origin to the outermost plane of atoms plus a "Gibbs distance" outside the surface; this is needed to properly achieve the transition from atomistic to continuum models.[24,58] Moreover, to obtain the correct limit with infinite size, the first term on the right must be such that the relevant energy terms scale linearly with the volume and also number of atoms. This is chosen here as the *definition* of the Gibb's cut used for each h_i, which in general leads to a nonlinear relationship between these and the number of atoms along specific directions. The continuum shape is then defined by the set of planes normal to all h_i, and all continuum quantities are defined via the appropriate partial derivatives or integrals taking care to include nonlinearity. We note that for most purposes the errors involved in the use of the equimolar cut will be small enough that the more general nonlinear forms can be avoided.

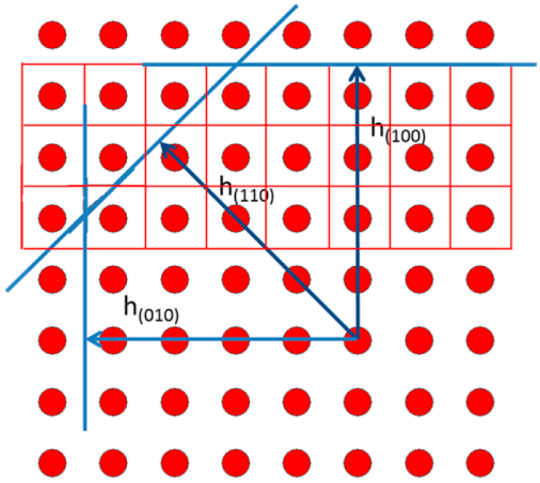

Figure 2. Equimolar surface partitioning based upon the Wigner−Seitz unit cells shown in red.

With this formulation, energy terms $O(h^3)$ are the bulk cohesive energy and strain energy terms, those of $O(h^2)$, the total surface free energy and surface stress terms (e.g., strain in MTPs), those of $O(h)$, the edge terms as well as counting corrections, and those of $O(h^0)$, the corner terms as well as additional counting corrections (e.g., to ensure the correct limit for a single atom). Note that this form automatically goes to the correct limit at large sizes and also (in principle if the Taylor series is expanded with terms $O(h^{-n})$) at small sizes; both limits need to be attained properly for the model to be valid. It is, however, crucial to understand the relative importance of the different terms when comparing nanoparticles with the same number of atoms, which generally follows Δ surface energy ≈ Δ strain energy > Δ surface stress energy in MTPs > Δ twin boundary energy ≈ Δ lattice parameter ≈ Δ counting corrections. For the purposes of this paper, we will ignore terms beyond $O(h^3)$ and $O(h^2)$, i.e., ignore the deviations at very small sizes (<2 nm). In the absence of tractions on the external surface of a nanoparticle (e.g., pressure), the $O(h^3)$ term contains the bulk cohesive energy as well as the energy associated with strain fields (which are critical for MTPs), i.e.,

$$\sum_{i,j,k} A_{ijk} h_i h_j h_k = V\left(\frac{\mu^B}{\nu_0} + W_D\right) \quad (3)$$

where V is the volume, μ^B, the bulk chemical potential, ν_0 the volume per atom, and W_D the strain energy density. We note that, in pressure-free systems, the total strain energy only depends upon the total volume. While energy models excluding the strain energy have been suggested,[42,59] these go to a physically incorrect limit at large sizes and are therefore necessarily incorrect. Additional terms can be added for pressure contributions, but these are small and cancel when different structures are compared.

The second term on the right of eq 2 can be written as

$$\sum_{i,j} B_{ij} h_i h_j = V^{2/3}(\gamma_{111}\varepsilon_w + \langle g_{ij} e_{ij}\rangle \varepsilon_g) \quad (4)$$

which contains the conventional surface free energy (γ) as well as that of twin boundaries in $V^{2/3}\gamma_{111}\varepsilon_w$ and the coupling between internal strains for MTPs and the surface free energy in $V^{2/3}\langle g_{ij} e_{ij}\rangle \varepsilon_g$, analyzed conventionally via the derivative of the surface free energy with respect to the in-plane strains in the surface $g_{ij} = d\gamma/de_{ij}$,[19,20,60] also called the surface stress tensor. In general, the difference in the total surface free energy between different nanoparticle shapes is much larger than the twin-boundary contributions; hence, the latter can be neglected for most fcc metals (typical twin boundary energies are no more than a few percent of surface free energies). Rigorously, the twin-boundary energies couple with the surface free energies in determining the final shape (e.g., refs 19 and 20), but this effect is small and can be neglected in most practical cases. Note that care needs to be taken with the definition of the reference states, as conventional elasticity theory uses the initial volume rather than a moving frame of reference.

To obtain the total energy, the volume and surface terms (eqs 3 and 4) are substituted in eq 2:

dx.doi.org/10.1021/jp401566m | J. Phys. Chem. C 2013, 117, 15859−15870

$$E = V\left(\frac{\mu^{B}}{v_0} + W_D\right) + V^{2/3}(\gamma_{111}\varepsilon_w + \langle g_{ij}e_{ij}\rangle\varepsilon_g) + O(h) \tag{5}$$

where the rightmost term includes any remaining corrections due to counting effects as well as edge and corner energies. For very small clusters (<2 nm), these may be important; otherwise, they can be safely neglected. In the absence of any strain terms, the minimum energy shape at constant volume is the variational minimum of ε_w (equivalently, the total energy at constant volume), and for a single crystal is given by the thermodynamic Wulff construction as the shape (set of points) S_w given by[61,62]

$$S_w = \{x\text{: } x.\ \hat{n} \le \lambda\gamma(\hat{n}) \text{ for all unit vectors } \hat{n}\} \tag{6}$$

The shape obtained thus contains all points x within $\hat{n} \le \lambda\gamma(\hat{n})$, where $\hat{n}$ is a unit vector defined by the crystallographic orientation of a face ($\{hkl\}$), $\gamma(\hat{n})$ is the orientation-dependent surface free energy, and λ is a constant that accounts for volume. Another common way to express this relationship is through the definition of the envelope planes of the particle, as first proved by Von Laue[5] and Dinghas:[6]

$$h_i = \lambda\gamma_i \tag{7}$$

where h_i is the normal distance from the center of the particle to a crystallographic facet i ($\{hkl\}$) as defined earlier, γ_i is the orientation-dependent surface free energy of the facet, and λ is defined as before. If the surface free energy is isotropic, the strain terms can become important, but for the faceted particles of interest herein, the coupling is a small third-order effect and will not be discussed further.

However, the thermodynamic shape will only be achieved if there is both time and energy available for bulk and/or surface diffusion processes to occur; this is rarely the case particularly for solution growth. Growth kinetics must thus be considered. An additional term can be defined, called the "weighted mean curvature" (wmc), the ratio of the change in surface energy (E_s) for a given facet (including surface stress contributions) and the change in volume (V):[63]

$$\begin{aligned}\mathrm{wmc}(h_i) &= \lim_{\delta\to 0} \Delta E_s(h_i + \delta h_i)/\Delta V(h_i + \delta h_i)\\ &= \mu^{s}(h_i)/v_0\end{aligned} \tag{8}$$

where $\mu^s(h_i)$ is the effective chemical potential associated with a given facet i as a function of h_i and v_0 is the atomic volume. Note that if four or more facets meet at a corner involving facet i some care is needed to distinguish limits for $\pm\delta$ due to the derivative discontinuity. For the thermodynamic Wulff shape, the weighted mean curvature is a constant for all h_i, an alternative description of equilibrium. It is worth mentioning that for faceted nanoparticles the weighted mean curvature is piecewise continuous and from solid geometry will scale with h_i as approximately

$$\mathrm{wmc}(h_i) = \overline{\gamma}_i/(L_i - h_i) \tag{9}$$

where the facet disappears for $h_i \ge L_i$ and eqs 8 and 9 define a weighted mean surface energy $\overline{\gamma}_i$. Note that this indicates that sharp corners are energetically unfeasible, rationalizing the fact that most experimental particles show at least some rounding.

In addition, since MTPs also contain strains with the strain energy density implicitly a functional of the shape, in principle, a fully rigorous description would include a term

$$\begin{aligned}w(h_i) &= \lim_{\delta\to 0} \Delta W_D(h_i + \delta h_i)/\Delta V(h_i + \delta h_i)\\ &= \mu^{w}(h_i)/v_0\end{aligned} \tag{10}$$

To date, there is no evidence that this shape-dependent strain energy contribution to the chemical potential matters for solution growth, although it is known to be important in epitaxial growth (e.g., refs 64−66). Neglecting this term, the differential equations for growth in the limit of no diffusion (of atoms within the particle) can then be written as a function of the chemical potential difference:

$$\frac{dh_i(t)}{dt} = v_i(\mu^{s}(h_i(t)) + \mu^{w}(h_i(t)) + \mu^{B} - \mu^{Ext}(t)) \tag{11}$$

where $\mu^{Ext}(t)$ is the relevant external chemical potential, assumed to be isotropic but not constant with time t. For simplicity, the bulk chemical potential is assumed to be time-invariant and local concentration gradients in the vicinity of the nanoparticle are neglected. In the special case when the growth velocity depends either weakly or linearly upon the chemical potential difference, a steady-state or Lyapunov solution exists for a single crystal as the shape S_K given by

$$S_K = \{x\text{: } x.\ \hat{n} \le \lambda(t)\nu(\hat{n}) \text{ for all unit vectors } \hat{n}\} \tag{12}$$

i.e., the shape corresponds to the inner envelope of planes normal to

$$h_i(t) = \lambda(t)v_i \tag{13}$$

This is called the "kinetic Wulff construction", and is deceptively similar to the Wulff construction with the critical difference that growth velocities (v) rather than the surface free energies (γ) determine the shape. In some cases, the shapes may be very similar, but there is no reason that they should be. For instance, the growth velocity in the presence of surfactants involves a number of kinetic processes such as activation energy barriers for atoms adding to the nanoparticle to diffuse through surfactant layers, as well as those for transition states where the surfactant is partially desorbed from the surface; in the thermodynamic case, the surface free energies only depend upon the ground state, equilibrium energies.

The thermodynamic and kinetic Wulff constructions represent the limits of very fast and very slow exchange of atoms between different surfaces, respectively. Since the exchange of atoms between different surfaces depends upon the difference in the weighted mean curvature, in the presence of some exchange of atoms between different faces, an approximate solution will be

$$h_i(t) \approx \lambda(t)v_i + \zeta(t)\mathrm{wmc}(h_i) \approx \lambda(t)v_i + \eta(t)\overline{\gamma}_i \tag{14}$$

where the vector of weighted mean curvatures and weighted surface free energies have been defined similar to before, and $\zeta(t)$ and $\eta(t)$ are scalar functions of time.

Both the thermodynamic and kinetic Wulff shapes have been extensively studied for single crystals, e.g., refs 7, 47−49, 61, 62, and 67−78. In some cases, softwares are available to calculate these shapes, for instance, for an isolated nanoparticle or one at an internal interface.[79,80] When the set of surface free energies in eq 4 is expanded to include an interface term, one arrives at the thermodynamic Winterbottom construction;[8] two interfaces yield the thermodynamic SummerTop construction.[9] For twin boundaries or by extension, other boundaries, the modified Wulff construction[19,20] can be used, with the addition that there is now a vector h_i for each single crystal subunit, and

that the scale term λ can be different for each subunit. Several analyses of growth on substrates assumed the growth velocity of the interface to be zero, e.g., refs 76−78, effectively using a kinetic Winterbottom construction. In the next sections, we will specifically discuss the kinetic version of the modified Wulff construction, including the important additional effects due to enhanced growth as a consequence of crystallographic defects. First, however, the results for the thermodynamic modified Wulff shape will be presented as a brief introduction to its kinetic variant.

THE MODIFIED WULFF CONSTRUCTION

To generate the shapes for twinned particles, the modified Wulff construction can be written as the superset of Wulff shapes S_m for all the individual single crystal subunits as follows

$$S_m = \{x: (x - o_m).\ \hat{n} \leq \lambda_m \gamma_m(\hat{n}) \text{ for all unit vectors } \hat{n}\} \tag{15}$$

where o_m is the origin for each single-crystal unit and $\gamma_m(\hat{n})$ is the surface free energy appropriately oriented in space, which includes a "twin facet" energy of $\alpha_{mn}\gamma_t$ for each segment "m" adjacent to a segment "n", with the additional conditions

$$S^t_{mn} = S^t_{nm} \quad \text{and} \quad \alpha_{mn} + \alpha_{nm} = 1 \tag{16}$$

where S^t_{mn} is the bounding twin surface of segment "m" where it joins to segment "n". Geometrically, this can be written as the following sequence of steps:

(1) Construct a Wulff polyhedron as per the standard Wulff construction for each single crystal subunit "m", including the twin boundaries as facets of free energy per unit area $\alpha_{mn}\gamma_t$, where γ_t is the twin boundary energy per unit area.
(2) Find the values of α_{mn} and the related segments such that the twin facet has identical geometry for adjacent units and the total twin-boundary energy is correctly counted.
(3) Assemble the segments to form a space-filling structure.

From the properties of the Wulff construction, for specified values of α_{mn} and λ_m, this is the global minimum total surface energy shape. With respect to variation in α_{mn} and λ_m, it may be a constrained local minimum in order to satisfy $S^t_{mn} = S^t_{nm}$ or a saddle point.

The simplest case is with $\alpha_{mn} = 1/2$ and all λ_m the same, i.e., the symmetric solution. One twin plane gives a singly twinned particle, while combining segments with parallel twin boundaries gives a family of LTPs, first observed in argon smokes.[38] Using five segments each bounded by two nonparallel planes gives a Dh; 20 segments bounded by three nonparallel boundaries, an Ic. Note that this leads to a family of structures defined by the number of twinned segments, not by the external surface. For instance, a regular icosahedron is obtained if only {111} and {100} facets are present; more complicated yet related structures arise if the {110} facets are of low energy.

By symmetry, it is simple to show that an equal partition is a stationary solution with respect to variation in α_{mn} and λ_m. Numerical calculations for a Dh yield a minimum for only {111} and {100} faceting,[33] although it is a saddle point for an isotropic surface free energy.[19,20] There is currently no analytical theory describing for what values of the surface free energy anisotropy the construction is a minimum versus a saddle point. Asymmetric partitioning of the twin boundary ($\alpha_{mn} \neq 1/2$) is also possible, in which case the scaling term λ_m for each segment is different. This leads to some of the asymmetric nanoparticle structures observed experimentally.[19]

For completeness, with clean surfaces, the twin-boundary energy is small compared to the surface free energies so it can be taken as zero (to first order approximation) for the geometric shape, in which case the origins o_m are common and this term can be removed. This approximation is accurate to second order in the energy,[19,20] and the difference in the shape will be below experimental error for vacuum or argon smoke experiments. From solid geometry, the total surface energy can be written (ignoring the twin boundary contribution) in terms of the parameter ε_w used in eq 4 as

$$\varepsilon_w = \left[\frac{9}{\gamma_{111}}\{N_1 S_1 + N_2 S_2\}\right]^{1/3} \tag{17}$$

where S_1 and S_2 are the integrated total surface free energies of the two regions R_1 and R_2 of the stereographic triangle in Figure 1 and N_1 and N_2, the numbers of each as mentioned previously.

For solvent-based growth, the surface free energies may be substantially lower, such that in some cases the coupling cannot be ignored and leads to re-entrant surfaces at the disclination line, as sometimes observed experimentally[81] and outlined in previous publications.[19,20]

As an example of how the modified Wulff construction can be used in a general fashion, consider a Dh with only {111} and {100} facets. If we assume that the surface energies are similar to those of a broken bond model[82] with $\gamma_{111}/\gamma_{100} = \sqrt{3}/2$ (inputs of eq 15), one gets the Marks decahedron with re-entrant surfaces at the twin boundaries (Figure 3a) as drawn in the original publications.[19,20] If the free energy of the {100} facets is decreased such that $\gamma_{111}/\gamma_{100} > 2/\sqrt{3}$, which can occur in the presence of stabilizing molecules such as surfactant (in the liquid phase) or chemisorbed species (in the gas phase), these notches disappear and the particle elongates to a rod-like shape similar to that first investigated by Ino[11−13] (Figure 3b).

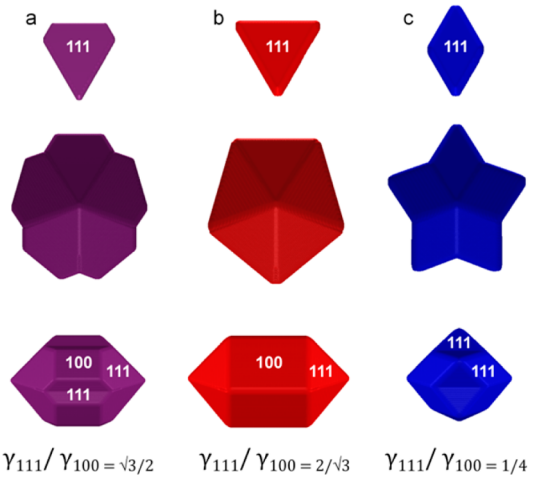

Figure 3. Thermodynamic Dh shape as a function of the relative surface free energy of {100} and {111} facets. (a) Re-entrant surfaces are obtained when the energy assumed is that of the broken bond model ($\gamma_{111}/\gamma_{100} = \sqrt{3}/2$). (b) Elongated decahedron/pentagonal rod without notches, obtained by lowering the {100} surface energy to $\gamma_{111}/\gamma_{100} = 2/\sqrt{3}$. (c) Star decahedron obtained by destabilizing the {100} facets ($\gamma_{111}/\gamma_{100} = 1/4$).

dx.doi.org/10.1021/jp401566m | J. Phys. Chem. C 2013, 117, 15859−15870

If instead the {100} energy is increased and becomes much larger than the {111} energy ($\gamma_{111}/\gamma_{100} \ll 1$), the {100} facets no longer appear in the minimal energy shape, and the result is a star decahedron (Figure 3c), similar to those recently synthesized by the Xia group.[83] Addition of {110} facets will lead to more rounded structures, as will inclusion of other higher index facets if these are of low enough surface free energy. Note that all these structures are related and all will contain a wedge disclination and/or strain-relieving dislocations; they only differ in which surfaces are of lowest energy. While they may have different properties, we argue that they should all be considered as members of a class of nanoparticles, not as different entities.

There are many more shapes that can be understood from the modified Wulff construction, for instance, variants of an Ic when {110} surfaces are low energy; these are simple to analyze and thus are not detailed here. While the modified Wulff construction has proved to be successful in rationalizing some observations, most notably for the Dh with re-entrant surface in the thermodynamically lowest energy shape, it does not explain everything. Perhaps the simplest shortcoming is a regular decahedron with only {111} facets. While these were described in the original papers on MTPs,[11−13] no thermodynamic argument will give their shape as a minimum energy configuration—that they are a minimum energy shape is a common misconception. Other shapes cannot be explained, such as sharp bipyramids, which have been synthesized using various protocols,[84−86] as well as truncated bitetrahedra, triangular platelets, and Dh rods. In many papers, these have been loosely attributed to "kinetics"; we now turn to put this on a firmer foundation.

THE KINETIC MODIFIED WULFF CONSTRUCTION

As introduced earlier, the shape when kinetics dominate may be related but is generally different from the thermodynamic shape; it depends upon the growth kinetics of different facets as well as the weighted mean curvature. Since the thermodynamic shapes when twin boundaries are present are no longer convex, the weighted mean curvature for the equilibrium shape no longer depends just upon the facet crystallography but depends upon whether the facet intersects the grain boundary or not. In addition, the re-entrant or concave surfaces that can exist are favorable attachment sites. All such factors need to be taken into account in order to model the kinetic shape of twinned nanoparticles.

The "kinetic modified Wulff construction" can be defined as the superset of the shapes for each segment of

$$S_m = \{x\text{: } x.\ \hat{n} \le \lambda(t)\nu_m(\hat{n}) \text{ for all unit vectors } \hat{n}\} \tag{18}$$

where the growth velocity of the twin boundaries has been taken as zero (assuming negligible bulk diffusion), a case which automatically satisfies the additional conditions of eq 14 as well as the different origins. Geometrically, this is equivalent to the following series of steps:

(1) Construct a kinetic Wulff polyhedron as per the standard kinetic Wulff construction but now using growth velocities and taking into account the enhanced growth for concave surfaces and facets adjacent to twin boundaries or other defects such as the disclination line in a Dh.
(2) Extract the appropriate volume for each segment bounded by twin boundaries, treating these as external facets of zero growth velocity.
(3) Assemble the segments to form a space-filling structure.

Specific forms for the enhancement will depend upon the precise experimental conditions and the type of shape considered. Here, such effects are parametrized via an enhancement of $\nu_m(\hat{n})$, more explicitly by multiplying it by 1 + $\varphi(\hat{n})$ for the relevant facets, where re-entrant surface, twin, and disclination enhancement contribute to $\varphi(\hat{n})$, i.e.,

$$\varphi(\hat{n}) = \varphi(\hat{n})_{\text{re-entrant}} + \varphi(\hat{n})_{\text{twin}} + \varphi(\hat{n})_{\text{disclination}} \tag{19}$$

For a re-entrant surface, only the faces that form the notch ({111}-type for Dh; {100}-type for LTP) are enhanced. Twin-enhanced growth involves enhancing any facet adjacent to the twin boundary, for example, both {111} and re-entrant {100} in a LTP. Lastly, disclination-assisted growth involves facets adjacent to the central disclinations in a Dh, i.e., the 10 {111} facets present in a perfect Dh. Note that disclination assisted growth for an Ic is also possible but in general will not give anything more than a regular Ic so will not be discussed further here. These terms were used to compute the kinetic Wulff shapes presented in this paper; more details are given in the Supporting Information.

An interesting example of kinetic growth is that of a Dh; as previously mentioned, the thermodynamic growth model fails to predict the sharp particles observed experimentally. The kinetic model succeeds, however. Indeed, if the growth rate of {100} facets is fast and there is enhanced growth at the re-entrant surfaces, a sharp, slightly elongated decahedron is formed (Figure 4b) instead of the thermodynamic Marks decahedron (Figure 4a). If, in addition to re-entrant growth enhancement, the {111} facet growth is slowed down (due to surfactants, for example), sharp pentagonal bipyramids are formed, similar to that commonly obtained experimentally (Figure 4c).[53,87−89] With enhanced re-entrant and disclination growth, rods are formed (Figure 4d) and depending upon which faces grow fast and slow there will be a range of end results, which is consistent with the many different reports in the literature.[87−97] Note that, similar to the thermodynamic

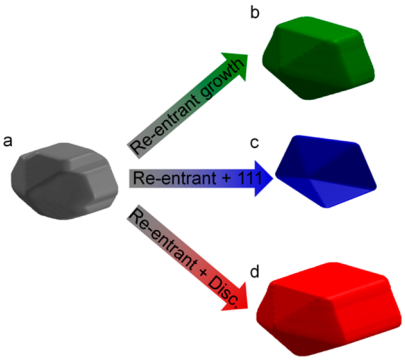

Figure 4. Effect of kinetic growth on Dh nanoparticles. All figures except part c have identical ν_{hkl} parameters equivalent to $\gamma_{111}/\gamma_{100} = \sqrt{3}/2$. A Marks decahedron (a) becomes a sharp Ino-like decahedron when re-entrant surface growth enhancement occurs ($\varphi_r > 0$, b), a pentagonal bipyramid when re-entrant growth and {111} surface stabilization occur ($\varphi_r > 0$, $\nu_{111}/\nu_{100} = 7/12$, c), and a perfect pentagonal rod when both kinetic enhancements occur ($\varphi_d > 0$, $\varphi_r > 0$, d).

dx.doi.org/10.1021/jp401566m | J. Phys. Chem. C 2013, 117, 15859−15870

shapes, these are not fundamentally different particles, just different yet related shapes one can obtain by varying the kinetics.

A second example is a LTP with a single twin, also referred to as a monotwin. Depending upon the conditions, a plethora of related shapes can be obtained, as illustrated in Figures 5 and 6.

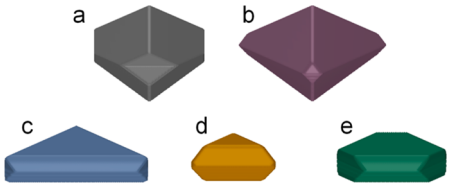

Figure 5. Singly twinned particle shapes obtained by varying the relative surface growth velocities and kinetic growth enhancements. (a) Particle with fast {111} growth and no kinetic enhancement, (b) sharp bipyramid obtained with fast {111} growth and kinetic enhancement at the re-entrant surfaces, (c) thin triangular platelet obtained with fast {100} growth and enhancement at both re-entrant surfaces and twin plane, (d) truncated bitetrahedron obtained with fast {100} growth and enhanced growth at the re-entrant surfaces, and (e) thin hexagonal platelet obtained with fast {100} growth and enhanced twin growth.

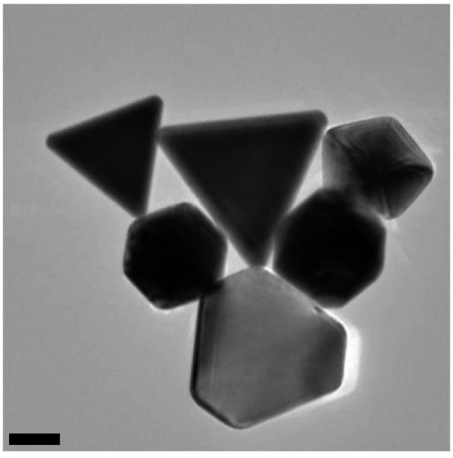

Figure 6. Reaction mixture from PVP-capped Au nanoparticles produced by reduction of hydrogen tetrachloroaurate ($HAuCl_4$).[53,54] Many of the shapes modeled by the modified kinetic Wulff construction are present: truncated bitetrahedra (top left and top middle), sharp decahedron (top right), icosahedra (middle left and middle right), and thin hexagonal platelet (bottom). The scale bar is 50 nm. Reprinted with permission from ref 55.

The structures in Figure 5b–e cannot be modeled with the thermodynamic Wulff construction. The thermodynamic shape for a monotwin with low {100} surface free energy (Figure 5a) becomes a sharp bipyramid (Figure 5b) when modeled with fast {111} growth (slow {100} growth, equivalent to low {100} surface free energy) and enhanced growth at the re-entrant surfaces. When modeled with fast {100} growth (slow {111} growth), a flat hexagon, truncated bitetrahedron, or flat triangular platelet can be obtained depending upon whether the enhancement is applied at the twin plane, the re-entrant surface, or both, respectively (Figure 5c–e).

Experimentally, sharp Ag bipyramids (Figure 5b) have been obtained in both PVP (poly(vinyl pyrrolidone)), a {100}-stabilizing surfactant[39,86,98,99] for Ag, and BSPP (bis-(*p*-sulfonatophenyl)phenylphosphine), a surfactant without strong preferential stabilization,[85,100,101] confirming the importance of kinetic control in this reaction.

The {111}-dominated monotwin particles modeled with the kinetic modified Wulff construction have also been widely observed in reaction products. Thick triangular structures, i.e., truncated bitetrahedra (Figure 5d), are produced under weak kinetic control and modeled with only a small enhancement at re-entrant surfaces, as is the case for perfect Dh (pentagonal bipyramids, Figure 4b). In fact, truncated bitetrahedra and perfect Dh are abundantly obtained with the same experimental growth conditions.[55,87] Interestingly, such synthesis also yields icosahedra and hexagonal plates. We show a representative image of a collection of PVP-capped nanoparticles containing various types of twins in Figure 6; PVP has been shown repeatedly to yield {111}-terminated Au particles[39,54,87,89,99,102–104] (unless Ag underpotential deposition is also present[39,54,102–105]). As discussed earlier, Ic emerge from seeds with 20 twin segments. The origin of hexagonal plates is not as straightforward, however. In our model, we can obtain this structure with fast {100} growth and enhanced twin growth (Figure 5e), meaning that all faces adjacent to the twin plane are growing equally fast. Following Lofton and Sigmund's framework for understanding re-entrant surfaces in thin plates,[106] this isotropy can occur in a particle with an even number of parallel twin planes; see also the earlier work on Argon smokes[38] for a larger database of simple twins and more crystallographies. Finally, thin triangular platelets (Figure 5c) have been known and studied for over a decade,[40,106–115] and kinetic control has been invoked repeatedly to explain their formation and fast degradation; in our model, strong kinetic enhancement (both at the twin and re-entrant surfaces) is indeed needed to obtain this shape.

DISCUSSION

The modified Wulff construction has been successful in explaining the thermodynamic shapes of fcc nanoparticles, and can without problem be used for other crystallographies. The modified kinetic Wulff construction provides a novel and useful framework for understanding particle shape, applicable to both liquid and gas phase growth as it holds whenever the particles do not change shape and surface diffusion or exchange through a solvent is slow compared to growth (as in most practical synthesis conditions). The agreement with experiments is excellent even at the simple level of parametrization of the surface growth rates of different surfaces with the important addition of additional enhancement terms for re-entrant surfaces and defects. In particular, this new model explains the presence of perfect Dh into the micrometer size regime in which they cannot be rationalized by thermodynamics, except for special cases such as when the constituent units are larger entities such as nanoparticles.[116]

The modified kinetic Wulff solution is different for each type of nanoparticles, for instance, monotwins versus MTPs. It follows that the relative rate of growth of different nanoparticle shapes will not be the same. Similar to the breakdown of the thermodynamics in terms of different regions of the stereographic triangle in Figure 1, the evolution of a population of nanoparticles of different shapes can be represented in terms of the relative growth rates of regions R_1 and R_2 as well as any kinetic enhancements due to the difference in the weighted mean curvature and growth enhancement effects at twin boundaries using a form similar to eq 17. If chemical etching occurs, it can lead to shape dependent Ostwald ripening, i.e.,

dx.doi.org/10.1021/jp401566m | J. Phys. Chem. C 2013, 117, 15859–15870

certain shapes shrink, whereas others grow, as has been well documented in cases of island growth (e.g., refs 64−66). This can obviously lead to shape selectivity. For instance, if a set of nuclei of single crystals and LTPs are initially present, the wmc for an odd number of twin boundaries (a stacking fault can be considered as two twin boundaries) may favor growth of triangular platelets, and size reduction of other shapes.

More formally, the differential equations for a population of nanoparticles can be described as

$$\frac{dV_i}{dt} = K(S_i, V_i, \mu^{Ext}) \tag{20}$$

where the rate of growth (or shrinkage) of particle "i" will depend upon its shape S_i, volume V_i, as well as the external chemical potential μ^{Ext} from liquid or gas phase atoms. As illustrated in Figure 7, depending upon the precise conditions,

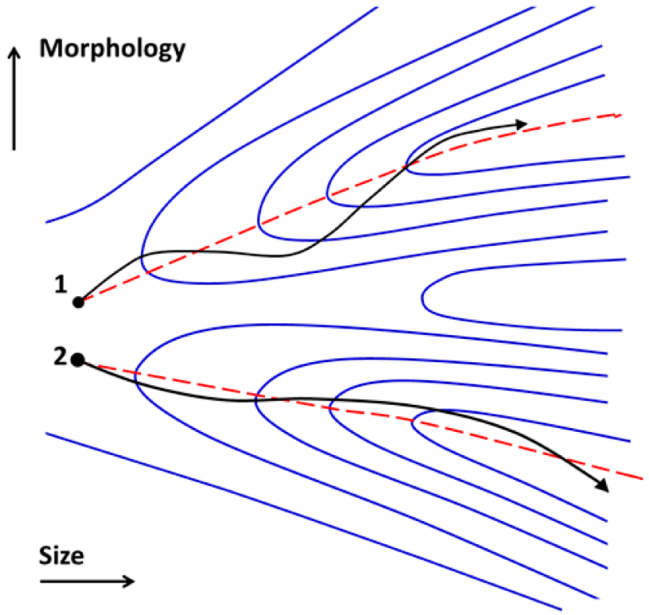

Figure 7. Growth kinetics diagram for two nanoparticles 1 and 2. The blue lines represent growth rate contours, the dashed red lines the Lyapunov solution, and the black lines the actual growth trajectories. At very small sizes, the population of each is in a statistical thermodynamic equilibrium. During growth, the morphology oscillates about the Lyapunov solution. In this case, nanoparticle 1 grows slower than 2; the exact details are strongly dependent upon the experimental growth conditions (temperature, time, chemical potentials, surfactants, etc.).

different nanoparticles will evolve at different rates, at any given time each approaching the appropriate kinetic or thermodynamic shape. This is why one frequently observes many different morphologies within the same reaction mixture, as for instance in Figure 6.

It is not hard to formulate the differential equations for growth including twins using, for instance, phase field methods with appropriate constraints to preserve the integrity of internal boundaries, and for different problems this has already been done. What is less than clear is exactly what are the values for the relevant reaction rates, nucleation rates, addition rates at step edges versus others as well as the chemical potentials in solution. While they could be treated as empirical parameters, experimental measurements would be desirable, as they could provide currently unavailable data. As an example, by obtaining careful high resolution electron microscopy measurements of the sharpness of the apexes of octahedra as a function of the chemical potential, it should be possible to quantify the role at small sizes of the weighted mean curvature via eq 9, in the limit of $h_i \rightarrow L_i$.

Some issues related to particle shape remain unaddressed. For applications, specific shapes should survive for days to years in use, and this raises issues about shape transitions. It is known that using surface diffusion rates extrapolated from high temperatures down to room temperature yields nanoparticle shape equilibration times of a few minutes; in reality, this does not occur, and the question of the barrier to shape transitions is still an open issue. Surface chemisorbed species may damp room temperature diffusion, and there may also be mechanistic transitions at low temperatures. Additionally, with isotropic surface free energies, no modified Wulff shape (i.e., twinned) is stable; they are at best metastable. When surface faceting is added, numerical calculations imply a barrier at least in a continuum model. Perhaps more significantly, motion of partial dislocations is necessary for the twins to move out of the particle, which requires too much activation energy at room temperature. Hence, as long as the temperature is low enough (nanoparticle equilibration is rapid based upon the epitaxial growth literature at around 200−300 °C) and surfactants or other species remain on the surface, the particle shape should be preserved. Note that this may not necessarily mean that kinetically grown nanoparticles will be of long-term use in most heterogeneous catalytic applications (especially at high temperatures), although additional stabilization techniques, such as epitaxy, can be employed.[117,118]

The kinetic model presented here may be oversimplified in some respects. Grouping the effects of defects and strain on the growth in a single enhancement factor is a reasonable first approximation, but the enhancement could in principle depend upon solution concentration for liquid-phase synthesis, or depend upon chemical potential gradients in a more exact model. This would be of interest for better modeling of nanoparticles on substrates, such as those used for heterogeneous catalysis. Velocity enhancements can be added to a kinetic Winterbottom[8] or Summertop[9] construction as was done for the kinetic modeling of two-dimensional island growth;[119] these follow the current modification directly, since there is no growth at the buried particle/substrate interface in most cases.

Careful, systematic electron microscopy analysis, proving (or disproving) size independence of shape as a function of the growth condition, would be the most useful data to move the field forward, providing insight into the underlying thermodynamic and kinetic contributions. In epitaxial growth, this was done some time ago to ensure commercially reproducible results; similar data for solution growth would greatly help the current understanding of nanoparticle growth.

CONCLUSION

A kinetic version of the modified Wulff construction was developed and used to successfully explain the plethora of different shapes obtained for twinned fcc materials. This model uses growth velocities and includes growth enhancement at favorable nucleation sites such as re-entrant surfaces and twin boundaries. The code and graphical user interface made available in the Supporting Information provide a useful teaching and research tool.

■ ASSOCIATED CONTENT

Supporting Information

Calculation details and parameters, graphical user interface files, and documentation. This material is available free of charge via the Internet at http://pubs.acs.org.

■ AUTHOR INFORMATION

Corresponding Author

*E-mail: er407@cam.ac.uk.

Present Address

[§]Department of Materials Science and Metallurgy, University of Cambridge, 27 Charles Babbage Road, Cambridge CB3 0FS, U.K.

Notes

The authors declare no competing financial interest.

Biographies

Emilie Ringe is the Gott Junior Research Fellow at Trinity Hall, Cambridge University, as well as a Newton International Research Fellow (the Royal Society, U.K.). She studied at McGill University at the undergraduate level before obtaining a MS from Northwestern University in inorganic crystallography with Professor James Ibers. She then completed a PhD in optical spectroscopy and analytical modeling of nanoparticle shape in the groups of Richard Van Duyne and Laurence Marks at Northwestern University in 2012. She currently works in the high resolution electron microscopy group at Cambridge University; her research interests include atomic resolution elemental mapping of alloy nanoparticles relevant for catalysis applications, as well as near-field plasmon mapping using electron energy loss spectroscopy.

Richard P. Van Duyne is the Charles E. and Emma H. Morrison Professor of Chemistry and Professor of Biomedical Engineering at Northwestern University. He received a BS (1967) at the Rensselaer Polytechnic Institute and PhD (1971) at the University of North Carolina, Chapel Hill, both in chemistry. He is a member of the National Academy of Sciences and the American Academy of Arts and Sciences. He is known for the discovery of surface-enhanced Raman spectroscopy (SERS), the invention of nanosphere lithography (NSL), and development of ultrasensitive nanosensors based on localized surface plasmon resonance (LSPR) spectroscopy.

Laurence D. Marks received his BA in chemistry and a PhD in physics from Cambridge University. Marks did postdoctoral training in Cambridge with Drs D. J. Smith and A. Howie as well as with Prof. J. M. Cowley at Arizona State University. Since 1985, he has been a faculty member at Northwestern University. He has research interests in a range of areas, from nanoparticles to nanotribology and surface science.

■ ACKNOWLEDGMENTS

This work was supported by the NSF (CHE-0911145) and the NSF MRSEC (DMR-1121262) at the Materials Research Center of Northwestern University. E.R. acknowledges support from Northwestern University in the form of a presidential fellowship. We thank Professors P. Voorhees and M. Asta for useful comments.

■ REFERENCES

(1) Gibbs, J. W. On the Equilibrium of Heterogeneous Substances. *Trans. Conn. Acad. Arts Sci.* **1874**, *3*, 343−524.

(2) Gibbs, J. W. On the Equilibrium of Heterogeneous Substances. *Trans. Conn. Acad. Arts Sci.* **1873**, *3*, 108−248.

(3) Gibbs, J. W. A Method of Geometrical Representation of the Thermodynamic Properties of Substances by Means of Surfaces. *Trans. Conn. Acad. Arts Sci.* **1873**, *2*, 382−404.

(4) Wulff, G. On the Question of Speed of Growth and Dissolution of Crystal Surfaces. *Z. Krystallogr.* **1901**, *34*, 449−530.

(5) von Laue, M. Der Wulffsche Satz fur die Gleichgewichtsform von Kristallen. *Z. Kristallogr.* **1943**, *105*, 124−133.

(6) Dinghas, A. Uber Einen Geometrischen Sat von Wulff fur die Gleichgewitchtsform von Kristallen. *Z. Kristallogr.* **1944**, *105*, 304−314.

(7) Herring, C. Some Theorems on the Free Energies of Crystal Surfaces. *Phys. Rev.* **1951**, *82*, 87−93.

(8) Winterbottom, W. L. Equilibrium Shape of a Small Particle in Contact with a Foreign Substrate. *Acta Metall. Mater.* **1967**, *15*, 303−310.

(9) Zia, R. K. P.; Avron, J. E.; Taylor, J. E. The Summertop Construction: Crystals in a Corner. *J. Stat. Phys.* **1988**, *50*, 727−736.

(10) Ringe, E.; Van Duyne, R. P.; Marks, L. D. Wulff Construction for Alloy Nanoparticles. *Nano Lett.* **2011**, *11*, 3399−3403.

(11) Ino, S. Epitaxial Growth of Metals on Rocksalt Faces Cleaved in Vacuum 2. Orientation and Structure of Gold Particles Formed in Ultrahigh Vacuum. *J. Phys. Soc. Jpn.* **1966**, *21*, 346−362.

(12) Ino, S.; Ogawa, S. Multiply Twinned Particles at Earlier Stages of Gold Film Formation on Alkalihalide Crystals. *J. Phys. Soc. Jpn.* **1967**, *22*, 1365−1374.
(13) Ino, S. Stability of Multiply-Twinned Particles. *J. Phys. Soc. Jpn.* **1969**, *27*, 941−953.
(14) Allpress, J. G.; Sanders, J. V. The Structure and Orientation of Crystals in Deposits of Metals on Mica. *Surf. Sci.* **1967**, *7*, 1−25.
(15) Komoda, T. Study on the Structure of Evaporated Gold Particles by Means of a High Resolution Electron Microscope. *Jpn. J. Appl. Phys.* **1968**, *7*, 27−30.
(16) Marks, L. D.; Smith, D. J. High-Resolution Studies of Small Particles of Gold and Silver 0.1. Multiply-Twinned Particles. *J. Cryst. Growth* **1981**, *54*, 425−432.
(17) Smith, D. J.; Marks, L. D. High-Resolution Studies of Small Particles of Gold and Silver 0.2. Single-Crystals, Lamellar Twins and Polyparticles. *J. Cryst. Growth* **1981**, *54*, 433−438.
(18) Hoare, M. R.; Pal, P. Statistics and Stability of Small Assemblies of Atoms. *J. Cryst. Growth* **1972**, *17*, 77−96.
(19) Marks, L. D. Modified Wulff Constructions for Twinned Particles. *J. Cryst. Growth* **1983**, *61*, 556−566.
(20) Marks, L. D. Surface-Structure and Energetics of Multiply Twinned Particles. *Philos. Mag. A* **1984**, *49*, 81−93.
(21) De Wit, R. Partial Disclinations. *J. Phys. C: Solid State Phys.* **1972**, *5*, 529−534.
(22) Howie, A.; Marks, L. D. Elastic Strains and the Energy-Balance for Multiply Twinned Particles. *Philos. Mag. A* **1984**, *49*, 95−109.
(23) Marks, L. D.; Smith, D. J. HREM and STEM of Defects in Multiply-Twinned Particles. *J. Microsc. (Oxford, U.K.)* **1983**, *130*, 249−261.
(24) Cleveland, C. L.; Landman, U. The Energetics and Structure of Nickel Clusters - Size Dependence. *J. Chem. Phys.* **1991**, *94*, 7376−7396.
(25) Cleveland, C. L.; Landman, U.; Luedtke, W. D. Phase Coexistence in Clusters. *J. Phys. Chem.* **1994**, *98*, 6272−6279.
(26) Müller, M.; Albe, K. Structural Stability of Multiply Twinned FePt Nanoparticles. *Acta Mater.* **2007**, *55*, 6617−6626.
(27) Baletto, F.; Ferrando, R. Structural Properties of Nanoclusters: Energetic, Thermodynamic, and Kinetic Effects. *Rev. Mod. Phys.* **2005**, *77*, 371−423.
(28) Yagi, K.; Takayanagi, K.; Kobayashi, K.; Honjo, G. In Situ Observations of Growth Processes of Multiply Twinned Particles. *J. Cryst. Growth* **1975**, *28*, 117−124.
(29) Iijima, S.; Ichihashi, T. Structural Instability of Ultrafine Particles of Metals. *Phys. Rev. Lett.* **1986**, *56*, 616−619.
(30) Ajayan, P. M.; Marks, L. D. Quasimelting and Phases of Small Particles. *Phys. Rev. Lett.* **1988**, *60*, 585−587.
(31) Ajayan, P. M.; Marks, L. D. Phase Instabilities in Small Particles. *Phase Transitions* **1990**, *24*−*26*, 229−258.
(32) Ajayan, P. M.; Marks, L. D. Experimental Evidence for Quasimelting in Small Particles. *Phys. Rev. Lett.* **1989**, *63*, 279−282.
(33) Dundurs, J.; Marks, L. D.; Ajayan, P. M. Structural Fluctuations in Small Particles. *Philos. Mag. A* **1988**, *57*, 605−620.
(34) Ball, K. D.; Berry, R. S.; Kunz, R. E.; Li, F.-Y.; Proykova, A.; Wales, D. J. From Topographies to Dynamics on Multidimensional Potential Energy Surfaces of Atomic Clusters. *Science* **1996**, *271*, 963−966.
(35) Berry, R. S. Potential Surfaces and Dynamics: What Clusters Tell Us. *Chem. Rev.* **1993**, *93*, 2379−2394.
(36) Cox, G.; Berry, R. S.; Johnston, R. L. Characterizing Potential Surface Topographies through the Distribution of Saddles and Minima. *J. Phys. Chem. A* **2006**, *110*, 11543−11550.
(37) Marks, L. D. Experimental Studies of Small-Particle Structures. *Rep. Prog. Phys.* **1994**, *57*, 603−649.
(38) Hayashi, T.; Ohno, T.; Yatsuya, S.; Uyeda, R. Formation of Ultrafine Metal Particles by Gas-Evaporation Technique 4. Crystal Habits of Iron and Fcc Metals, Al, Co, Ni, Cu, Pd, Ag, In, Au and Pb. *Jpn. J. Appl. Phys.*, **1997**, *16*.
(39) Xia, Y.; Xiong, Y.; Lim, B.; Skrabalak, S. E. Shape-Controlled Synthesis of Metal Nanocrystals: Simple Chemistry Meets Complex Physics? *Angew. Chem., Int. Ed.* **2009**, *48*, 60−103.
(40) Jin, R.; Cao, Y. C.; Hao, E.; Métraux, G. S.; Schatz, G. C.; Mirkin, C. A. Controlling Anisotropic Nanoparticle Growth through Plasmon Excitation. *Nature* **2003**, *425*, 487−490.
(41) Xiong, Y.; Wiley, B. J.; Xia, Y. Nanocrystals with Unconventional Shapes– a Class of Promising Catalysts. *Angew. Chem., Int. Ed.* **2007**, *46*, 7157−7159.
(42) Barnard, A. S.; Young, N. P.; Kirkland, A. I.; van Huis, M. A.; Xu, H. F. Nanogold: A Quantitative Phase Map. *ACS Nano* **2009**, *3*, 1431−1436.
(43) Young, N. P.; van Huis, M. A.; Zandbergen, H. W.; Xu, H.; Kirkland, A. I. Transformations of Gold Nanoparticles Investigated Using Variable Temperature High-Resolution Transmission Electron Microscopy. *Ultramicroscopy* **2010**, *110*, 506−516.
(44) Dorogin, L. M.; Vlassov, S.; Kolesnikova, A. L.; Kink, I.; Lohmus, R.; Romanov, A. E. Crystal Mismatched Layers in Pentagonal Nanorods and Nanoparticles. *Phys. Status Solidi B* **2010**, *247*, 288−298.
(45) Patala, S.; Marks, L. D.; Olvera de la Cruz, M. Elastic Strain Energy Effects in Faceted Decahedral Nanoparticles. *J. Phys. Chem. C* **2013**, *117*, 1485−1494.
(46) Frank, F. C. In *Growth and Perfection of Crystals*; Doremus, R. H., Roberts, B. W., Tumbull, D., Eds.; Wiley: New York, 1958.
(47) Villain, J. Nonequilibrium Systems - The Shape of Crystals to Come. *Nature* **1991**, *350*, 273−274.
(48) Sekerka, R. F. Equilibrium and Growth Shapes of Crystals: How Do They Differ and Why Should We Care? *Cryst. Res. Technol.* **2005**, *40*, 291−306.
(49) Taylor, J. E.; Cahn, J. W.; Handwerker, C. A. Overview No. 98 1- Geometric Models of Crystal-Growth. *Acta Metall. Mater.* **1992**, *40*, 1443−1474.
(50) Gorshkov, V.; Zavalov, A.; Privman, V. Shape Selection in Diffusive Growth of Colloids and Nanoparticles. *Langmuir* **2009**, *25*, 7940−7953.
(51) Wettlaufer, J. S.; Jackson, M.; Elbaum, M. A Geometric Model for Anisotropic Crystal Growth. *J. Phys. A: Math. Gen.* **1994**, *27*, 5957−5967.
(52) Jindal, V.; Shahedipour-Sandvik, F. Theoretical Prediction of GaN Nanostructure Equilibrium and Nonequilibrium Shapes. *J. Appl. Phys.* **2009**, *106*, 083115.
(53) Seo, D.; Yoo, C. I.; Chung, I. S.; Park, S. M.; Ryu, S.; Song, H. Shape Adjustment between Multiply Twinned and Single-Crystalline Polyhedral Gold Nanocrystals: Decahedra, Icosahedra, and Truncated Tetrahedra. *J. Phys. Chem. C* **2008**, *112*, 2469−2475.
(54) Langille, M. R.; Zhang, J.; Mirkin, C. A. Plasmon-Mediated Synthesis of Heterometallic Nanorods and Icosahedra. *Angew. Chem., Int. Ed.* **2011**, *50*, 3543−3547.
(55) Ringe, E.; Langille, M. R.; Sohn, K.; Zhang, J.; Huang, J.; Mirkin, C. A.; Van Duyne, R. P.; Marks, L. D. Plasmon Length: A Universal Parameter to Describe Size Effects in Gold Nanoparticles. *J. Phys. Chem. Lett.* **2012**, *3*, 1479−1483.
(56) Batyrev, I.; Alavi, A.; Finnis, M. W. Ab Initio Calculations on the Al_2O_3(0001) Surface. *Faraday Discuss.* **1999**, *114*, 33−43.
(57) Reuter, K.; Scheffler, M. Composition, Structure, and Stability of RuO_2(110) as a Function of Oxygen Pressure. *Phys. Rev. B* **2002**, 65.
(58) Hamilton, J. C. Edge Energies: Atomistic Calculations of a Continuum Quantity. *Phys. Rev. B* **2006**, *73*, 125447.
(59) Barnard, A. S. Modelling of Nanoparticles: Approaches to Morphology and Evolution. *Rep. Prog. Phys.* **2010**, *73*, 086502.
(60) Howie, A.; Marks, L. D. Elastic Strains and the Energy-Balance for Multiply Twinned Particles. *Philos. Mag. A* **1984**, *49*, 95−109.
(61) Cahn, J. W.; Hoffman, D. W. Vector Thermodynamics for Anisotropic Surfaces 2. Curved and Faceted Surfaces. *Acta Metall. Mater.* **1974**, *22*, 1205−1214.
(62) Hoffman, D. W.; Cahn, J. W. Vector Thermodynamics for Anisotropic Surfaces 1. Fundamentals and Application to Plane Surface Junctions. *Surf. Sci.* **1972**, *31*, 368−388.

(63) Taylor, J. E. Overview No. 98 2- Mean-Curvature and Weighted Mean-Curvature. *Acta Metall. Mater.* **1992**, *40*, 1475−1485.
(64) Drucker, J. Coherent Islands and Microstructural Evolution. *Phys. Rev. B* **1993**, *48*, 18203−18206.
(65) Hammar, M.; LeGoues, F. K.; Tersoff, J.; Reuter, M. C.; Tromp, R. M. In Situ Ultrahigh Vacuum Transmission Electron Microscopy Studies of Hetero-Epitaxial Growth 1. Si(001)/Ge. *Surf. Sci.* **1996**, *349*, 129−144.
(66) Ross, F. M.; Tersoff, J.; Tromp, R. M. Coarsening of Self-Assembled Ge Quantum Dots on Si(001). *Phys. Rev. Lett.* **1998**, *80*, 984−987.
(67) Cahn, J. W.; Taylor, J. E. A Contribution to the Theory of Surface-Energy Minimizing Shapes. *Scr. Metall. Mater.* **1984**, *18*, 1117−1120.
(68) Cahn, J. W.; Carter, W. C. Crystal Shapes and Phase Equilibria: A Common Mathematical Basis. *Metall. Mater. Trans. A* **1996**, *27*, 1431−1440.
(69) Coriell, S. R.; Sekerka, R. F. Effect of Anisotropy of Surface-Tension and Interface Kinetics on Morphological Stability. *J. Cryst. Growth* **1976**, *34*, 157−163.
(70) Uehara, T.; Sekerka, R. F. Phase Field Simulations of Faceted Growth for Strong Anisotropy of Kinetic Coefficient. *J. Cryst. Growth* **2003**, *254*, 251−261.
(71) Almgren, F.; Taylor, J. E.; Wang, L. Curvature-Driven Flows - A Variational Approach. *Siam J. Control Optim.* **1993**, *31*, 387−437.
(72) Cahn, J. W.; Taylor, J. E. Overview No-113 - Surface Motion by Surface-Diffusion. *Acta Metall. Mater.* **1994**, *42*, 1045−1063.
(73) Carter, W. C.; Roosen, A. R.; Cahn, J. W.; Taylor, J. E. Shape Evolution by Surface-Diffusion End Surface Attachment Limited Kinetics on Completely Faceted Surfaces. *Acta Metall. Mater.* **1995**, *43*, 4309−4323.
(74) Ambrosio, L.; Soner, H. M. Level Set Approach to Mean Curvature Flow in Arbitrary Codimension. *J. Diff. Geom.* **1996**, *43*, 693−737.
(75) Winn, D.; Doherty, M. F. Modeling Crystal Shapes of Organic Materials Grown from Solution. *AIChE J.* **2000**, *46*, 1348−1367.
(76) Du, D. X.; Srolovitz, D. J.; Coltrin, M. E.; Mitchell, C. C. Systematic Prediction of Kinetically Limited Crystal Growth Morphologies. *Phys. Rev. Lett.* **2005**, *95*, 155503.
(77) Sun, Q.; Yerino, C. D.; Ko, T. S.; Cho, Y. S.; Lee, I. H.; Han, J.; Coltrin, M. E. Understanding Nonpolar GaN Growth through Kinetic Wulff Plots. *J. Appl. Phys.* **2008**, *104*, 093523.
(78) Leung, B.; Sun, Q.; Yerino, C. D.; Han, J.; Coltrin, M. E. Using the Kinetic Wulff Plot to Design and Control Nonpolar and Semipolar GaN Heteroepitaxy. *Semicond. Sci. Technol.* **2012**, *27*, 024005.
(79) Zucker, R.; Chatain, D.; Dahmen, U.; Hagège, S.; Carter, W. C. New Software Tools for the Calculation and Display of Isolated and Attached Interfacial-Energy Minimizing Particle Shapes. *J. Mater. Sci.* **2012**, *47*, 1−13.
(80) Roosen, A. R.; McCormack, R. P.; Carter, W. C. Wulffman: A Tool for the Calculation and Display of Crystal Shapes. *Comput. Mater. Sci.* **1998**, *11*, 16−26.
(81) Hofmeister, H. Shape Variations and Anisotropic Growth of Multiply Twinned Nanoparticles. *Z. Kristallogr.* **2009**, *224*, 528−538.
(82) Marks, L. D. Particle Size Effects on Wulff Constructions. *Surf. Sci.* **1985**, *150*, 358−366.
(83) Lim, B.; Wang, J.; Camargo, P. H. C.; Cobley, C. M.; Kim, M. J.; Xia, Y. Twin-Induced Growth of Palladium−Platinum Alloy Nanocrystals. *Angew. Chem., Int. Ed.* **2009**, *48*, 6304−6308.
(84) McEachran, M.; Kitaev, V. Direct Structural Transformation of Silver Platelets into Right Bipyramids and Twinned Cube Nanoparticles: Morphology Governed by Defects. *Chem. Commun.* **2008**, 5737−5739.
(85) Zhang, J.; Li, S.; Wu, J.; Schatz, G. C.; Mirkin, C. A. Plasmon-Mediated Synthesis of Silver Triangular Bipyramids. *Angew. Chem., Int. Ed.* **2009**, *48*, 7787−7791.
(86) Wiley, B. J.; Xiong, Y.; Li, Z.-Y.; Yin, Y.; Xia, Y. Right Bipyramids of Silver: A New Shape Derived from Single Twinned Seeds. *Nano Lett.* **2006**, *6*, 765−768.
(87) Sánchez-Iglesias, A.; Pastoriza-Santos, I.; Pérez-Juste, J.; Rodríguez-González, B.; García de Abajo, F. J.; Liz-Marzán, L. M. Synthesis and Optical Properties of Gold Nanodecahedra with Size Control. *Adv. Mater.* **2006**, *18*, 2529−2534.
(88) Pastoriza-Santos, I.; Sánchez-Iglesias, A.; García de Abajo, F. J.; Liz-Marzán, L. M. Environmental Optical Sensitivity of Gold Nanodecahedra. *Adv. Funct. Mater.* **2007**, *17*, 1443−1450.
(89) Rodríguez-Fernández, J.; Novo, C.; Myroshnychenko, V.; Funston, A. M.; Sánchez-Iglesias, A.; Pastoriza-Santos, I.; Pérez-Juste, J.; García de Abajo, F. J.; Liz-Marzán, L. M.; Mulvaney, P. Spectroscopy, Imaging, and Modeling of Individual Gold Decahedra. *J. Phys. Chem. C* **2009**, *113*, 18623−18631.
(90) Pietrobon, B.; Kitaev, V. Photochemical Synthesis of Monodisperse Size-Controlled Silver Decahedral Nanoparticles and Their Remarkable Optical Properties. *Chem. Mater.* **2008**, *20*, 5186−5190.
(91) Du, Y. K.; Xu, J. Z.; Shen, M.; Yang, P.; Jiang, L. Alkanethiol-Stabilized Decahedron of Gold Nanoparticles. *Colloids Surf., A* **2005**, *257−258*, 535−537.
(92) Sun, Y.; Gates, B.; Mayers, B.; Xia, Y. Crystalline Silver Nanowires by Soft Solution Processing. *Nano Lett.* **2002**, *2*, 165−168.
(93) Pietrobon, B.; McEachran, M.; Kitaev, V. Synthesis of Size-Controlled Faceted Pentagonal Silver Nanorods withTunable Plasmonic Properties and Self-Assembly of These Nanorods. *ACS Nano* **2009**, *3*, 21−26.
(94) Reyes-Gasga, J.; Elechiguerra, J. L.; Liu, C.; Camacho-Bragado, A.; Montejano-Carrizales, J. M.; Yacaman, M. J. On the Structure of Nanorods and Nanowires with Pentagonal Cross-Sections. *J. Cryst. Growth* **2006**, *286*, 162−172.
(95) Hofmeister, H.; Nepijko, S. A.; Ievlev, D. N.; Schulze, W.; Ertl, G. Composition and Lattice Structure of Fivefold Twinned Nanorods of Silver. *J. Cryst. Growth* **2002**, *234*, 773−781.
(96) Canizal, G.; Ascencio, J. A.; Gardea-Torresday, J.; Yacaman, M. J. Multiple Twinned Gold Nanorods Grown by Bio-Reduction Techniques. *J. Nanopart. Res.* **2001**, *3*, 475−481.
(97) Ni, C.; Hassan, P. A.; Kaler, E. W. Structural Characteristics and Growth of Pentagonal Silver Nanorods Prepared by a Surfactant Method. *Langmuir* **2005**, *21*, 3334−3337.
(98) Lu, X.; Rycenga, M.; Skrabalak, S. E.; Wiley, B. J.; Xia, Y. Chemical Synthesis of Novel Plasmonic Nanoparticles. *Annu. Rev. Phys. Chem.* **2009**, *60*, 167−192.
(99) Sun, Y.; Xia, Y. Shape-Controlled Synthesis of Gold and Silver Nanoparticles. *Science* **2002**, *298*, 2176−2179.
(100) Zhang, J.; Langille, M. R.; Mirkin, C. A. Photomediated Synthesis of Silver Triangular Bipyramids and Prisms: The Effect of pH and BSPP. *J. Am. Chem. Soc.* **2010**, *132*, 12502−12510.
(101) Ringe, E.; Zhang, J.; Langille, M. R.; Mirkin, C. A.; Marks, L. D.; Van Duyne, R. P. Correlating the Structure and Localized Surface Plasmon Resonance of Single Silver Right Bipyramids. *Nanotechnology* **2012**, *23*, 444005.
(102) Wiley, B. J.; Im, S. H.; Li, Z.-Y.; McLellen, J.; Siekkinen, A.; Xia, Y. Maneuvering the Surface Plasmon Resonance of Silver Nanostructures through Shape-Controlled Synthesis. *J. Phys. Chem. B* **2006**, *110*, 15666−15675.
(103) Kim, F.; Connor, S.; Song, H.; Kuykendall, T.; Yang, P. Platonic Gold Nanocrystals. *Angew. Chem.* **2004**, *116*, 3759−3763.
(104) Grzelczak, M.; Pérez-Juste, J.; Mulvaney, P.; Liz-Marzán, L. M. Shape Control in Gold Nanoparticle Synthesis. *Chem. Soc. Rev.* **2008**, *37*, 1783−1791.
(105) Personick, M. L.; Langille, M. R.; Zhang, J.; Mirkin, C. A. Shape Control of Gold Nanoparticles by Silver Underpotential Deposition. *Nano Lett.* **2011**, *11*, 3394−3398.
(106) Lofton, C.; Sigmund, W. Mechanisms Controlling Crystal Habits of Gold and Silver Colloids. *Adv. Funct. Mater.* **2005**, *15*, 1197−1208.
(107) Munechika, K.; Smith, J. M.; Chen, Y.; Ginger, D. S. Plasmon Line Widths of Single Silver Nanoprisms as a Function of Particle Size and Plasmon Peak Position. *J. Phys. Chem. C* **2007**, *111*, 18906−18911.

(108) Pastoriza-Santos, I.; Liz-Marzán, L. M. Colloidal Silver Nanoplates. State of the Art and Future Challenges. *J. Mater. Chem.* **2008**, *18*, 1724−1737.
(109) Sherry, L. A.; Jin, R.; Mirkin, C. A.; Schatz, G. C.; Van Duyne, R. P. Localized Surface Plasmon Resonance Spectroscopy of Single Silver Triangular Nanoprisms. *Nano Lett.* **2006**, *6*, 2060−2065.
(110) Jin, R.; Cao, Y.; Mirkin, C. A.; Kelly, K. L.; Schatz, G. C.; Zheng, J. G. Photoinduced Conversion of Silver Nanospheres to Nanoprisms. *Science* **2001**, *294*, 1901−1903.
(111) Nelayah, J.; Kociak, M.; Stéphan, O.; Geuquet, N.; Henrard, L.; García de Abajo, F. J.; Pastoriza-Santos, I.; Liz-Marzán, L. M.; Colliex, C. Two-Dimensional Quasistatic Stationary Short Range Surface Plasmons in Flat Nanoprisms. *Nano Lett.* **2010**, *10*, 902−907.
(112) Nelayah, J.; Kociak, M.; Stéfan, O.; García de Abajo, F. J.; Tencé, M.; Henrard, L.; Taverna, D.; Pastoriza-Santos, I.; Liz-Marzán, L. M.; Colliex, C. Mapping Surface Plasmons on a Single Metallic Nanoparticle. *Nat. Phys.* **2007**, *3*, 348−353.
(113) Kirkland, A. I.; Edwards, P. P.; Jefferson, D. A.; Duff, D. G. The Structure, Characterization, and Evolution of Colloidal Metals. *Annu. Rep. Prog. Chem., Sect. C: Phys. Chem.* **1990**, *87*, 247−304.
(114) Rocha, T. C. R.; Zanchet, D. Structural Defects and Their Role in the Growth of Ag Triangular Nanoplates. *J. Phys. Chem. C* **2007**, *111*, 6989−6993.
(115) Blaber, W. G.; Henri, A.-I.; Bingham, J.; Schatz, G. C.; Van Duyne, R. P. LSPR Imaging of Silver Triangular Nanoprisms: Correlating Scattering with Structure Using Electrodynamics for Plasmon Lifetime Analysis. *J. Phys. Chem. C* **2012**, *116*, 393−403.
(116) Rupich, S. M.; Shevchenko, E. V.; Bodnarchuk, M. I.; Lee, B.; Talapin, D. V. Size-Dependent Multiple Twinning in Nanocrystal Superlattices. *J. Am. Chem. Soc.* **2010**, *132*, 289−296.
(117) Enterkin, J. A.; Setthapu, W.; Elam, J. W.; Christensen, S. T.; Rabuffetti, F. A.; Marks, L. D.; Stair, P. C.; Poeppelmeier, K. R.; Marshall, C. L. Propane Oxidation over $Pt/SrTiO_3$ Nanocuboids. *ACS Catal.* **2011**, *1*, 629−635.
(118) Enterkin, J. A.; Poeppelmeier, K. R.; Marks, L. D. Oriented Catalytic Platinum Nanoparticles on High Surface Area Strontium Titanate Nanocuboids. *Nano Lett.* **2011**, *11*, 993−997.
(119) Berge, B.; Faucheux, L.; Schwab, K.; Libchaber, A. Faceted Crystal Growth in Two Dimensions. *Nature* **1991**, *350*, 322−324.